Taylor & Francis
Taylor & Francis Group

Check for updates

ORIGINAL ARTICLE

Modelling and FEM simulation of a rotating hyperelastic spherical balloon actuator

Vinod Yadav[a], Deepak Kumar [ID][a], Ayush Srivastav[a] and Somnath Sarangi[b]

[a]Department of Mechanical Engineering, Maulana Azad National Institute of Technology Bhopal, Bhopal, India; [b]Department of Mechanical Engineering, Indian Institute of Technology Patna, India

ABSTRACT

This paper presents static modelling and simulation of a spherically-shaped hyperelastic balloon actuator subjected to an angular rotation with an internally applied air pressure. These actuators are extensively used in soft robotics because its safe and flexible nature. The balloon actuator is a pneumatic-type actuator made of a polymeric material. A continuum mechanics-based analytical modelling and Finite element method-based simulation are performed to predict the response of the actuator for a given angular rotation with internally applied air pressure. The proposed modelling framework is subsequently utilised to perform the parametric studies for varying pressure, thickness, and rotational speed of the actuator. Various elastic instability curves are also obtained to examine the critical inflation of the rubber balloon actuator. The analytical findings agree well with the FEM simulations.

1. Introduction

In the current scenario, the research on soft material mechanics (Treloar 1974, 1976) has gained significant attention with the advent of the soft robotics field (Albu-Schäffer et al. 2008; Verl et al. 2015). Soft material mechanics always deals with the fundamental principle of continuum mechanics that can potentially solve the new generation complex systems with advanced computational methods. Advances in continuum mechanics have currently renewed interest in finite element modelling of rubber-like materials (Nicholson and Nelson 1990; Moskvichev, Porokhin, and Shcherbakov 2017) for the quick material response calculations under the applied load. The rubber-like materials are used to design various actuators used in different engineering and medical fields (Ashwin and Ghosal 2019; Kumar et al. 2021). The high nonlinearity in stress–strain behaviour of rubber-like materials can encounter mathematical difficulties in the continuum mechanics to get the quick actuator responses made of such materials. A coupled continuum mechanics-based FEM modelling approach (Valavala and Odegard 2021) overcomes this challenge. In general, the rubber-like materials fall under an incompressible, isotropic, and hyperelastic material class as per the theory of nonlinear elasticity, one of the continuum mechanics branches. Also, these rubber-like materials undergo large deformations that can exhibit a variety of elastic instabilities (Gent 2005; Wang et al. 2018).

Our concern here is with one of the classical problems of a rubber balloon actuator (Beatty 1987) that is internally pressurised with applied air pressure. A similar problem is explored here with an additional rotational effect. The rotating rubber balloon actuator with an internally applied pressure will have various upcoming engineering and medical applications, specifically in the soft robotic field. In this context, a pendulum-based spherical rolling robot with a softshell (Sheng et al. 2014) shown in Figure 1 is designed to meet the needs of attitude stabilisation and control for the robot.

Some of the application-based earlier works on the pneumatic balloon actuator dealt with designing human-friendly actuation systems. These works mainly dealt with a human-friendly actuation system design and control of the leading-edge vortices of a delta wing (Lee et al. 1998) and the rehabilitation robots (Noritsugu 1999). In line with that, Jeong et al. (Jeong, Kusuda, and Konishi 2005; Jeong et al. 2005) designed a pneumatic micro-finger based on the balloon actuator system and achieved the finger's bidirectional motion. Similarly, an articulated micro-finger to construct the micro-robotic end-effectors such as micro-hand was developed by Lu and Kim (Lu and Kim 2003a) and characterised by the same authors (Lu and Kim 2003b). Further, Saga et al. (Saga, Nagase, and Saikawa 2005) developed a gentle robotic tendon for nursing medical patients using a pneumatic balloon. In view of the rubber-like material modelling aspects, including balloon actuator system, a well-known study was presented by Beatty (Beatty 1987).
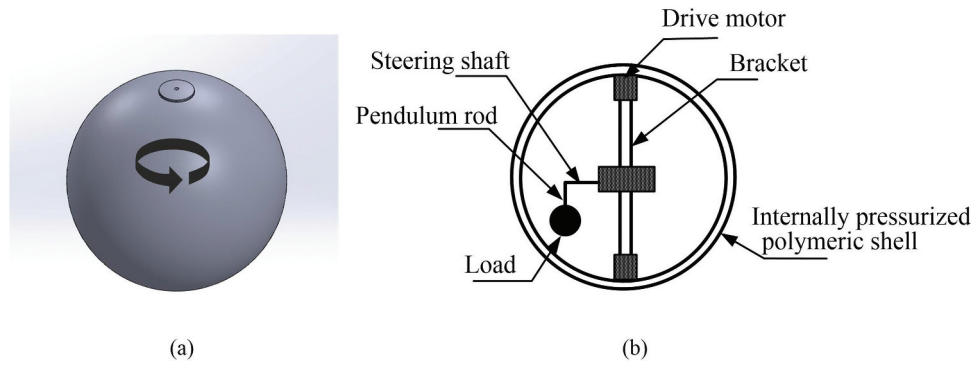
CONTACT Deepak Kumar ✉ deepakkumaromre@manit.ac.in

Figure 1. Outer and inner planform of a spherical soft shell robot: (a) Outer planform (b) Inner planform.

This study surveyed the topics in finite elasticity focussed on the modelling of classical experimental works by Rivlin and Saunders (Rivlin 1948, 1949), a famous Blatz and Ko experiment (Blatz and Ko 1962), and the biological tissue experiments performed by Fung (Fung 1967). The earlier studies (Alexander 1971; Needleman 1977; Ogden 1982) on the modelling of pneumatic balloon actuator dealt with the inflation phenomenon of the actuator with applied air pressure. A common observation was highlighted that the onset of highly non-uniform deformations in the inflated balloon actuators has profound implications. In line with that, Gent (Gent 2005) modelled the novel instabilities that occurred in the inflated balloon actuator undergoing the large deformations. Similarly, a pear-shaped bifurcation and the localised bulging phenomena were modelled by Wang (Wang et al. 2018). Further, Kanner and Horgan (Kanner and Horgan 2007) investigated the strain-stiffening effect in the inflated thin balloon actuator's stress-stretch response targeting the biomedical field of applications. Mao et al. (Mao et al. 2014) studied the effect of pre-stretching on the balloon actuator's instability and observed a significant instability suppression during inflation. Furthermore, Zamani and Pence (Zamani and Pence 2017) modelled the swelling-burst instability in the balloon actuator by obtaining the monotonic pressure versus radius-based instability curves to examine the critical inflation. ZhiYong and Yenwen (An and Lu 2005) developed a finite elasticity-based numerical model to predict a pneumatic balloon-jointed actuation criticality utilised in the micro-hand to perform an out-of-plane rotation.

n light of the current developments of the balloon actuator, Andersen and Hansen (Andersen and Hansen 2005) showed how modelling and simulation could be used to analyse and design actuators with fluid power actuation. Further, Hwang et al. (Hwang, Paydar, and Candler 2015) developed and modelled a unique balloon fin actuator design to produce a linear bend angle change

with pressurised air injection. Simon and Carraro (Simon and Carraro 2019) performed a two-balloon experiment connecting two rubber balloons by allowing them to exchange gas together. They observed that the discrepancy of balloon size between the two (meta)stable states decreases and, beyond, bistability is impossible. Furthermore, He et al. (He et al. 2020) studied anomalous inflation of a nematic balloon by observing that the balloon contracts significantly along its axial direction with a small increment of inflating pressure while expanding in its radial direction. At last, Jebur et al. (Jebur, Jweeg, and Al-Waily 2021) characterised and simulated the mechanical properties of pphr rubber, extensively used in different engineering applications, including balloon actuators.

Many investigators scrutinised the hyperelasticity-based analytical solutions of an internally pressurised balloon actuator made of rubber-like material. They combined the analytical solution-based mathematical challenges with well-established numerical simulations to analyse the actuator response. Motivated by them, the present paper explores a similar problem with an additional rotational effect on the rubber balloon actuator. In general, the rotational effect is predominant in the soft robotic arm while it is undergoing rotation. In most of the previous works, the rotational motion is not considered.

The current study aims at a thermodynamically consistent and FEM simulation-based model solution to predict the deformation response of a rubber balloon actuator for an internally applied air pressure for a given rotation. A systematic continuum mechanics-based modelling framework with well-established computational techniques is adopted to solve the problem. The study also aims to verify the findings of the developed model with FEM simulations. As a result, the radial and circumferential or hoop stress distributions of the actuator at different rotational inputs, different internal pressures, and different initial thicknesses are plotted. At last, various elastic instability curves are plotted to examine the critical inflation of the actuator.

The outline of the paper is as follows: In Section 2, the theoretical model for the aforementioned problem is developed. In Section 3, the finite element method-based analysis for the problem is presented. In Section 4, several analytical and simulation findings of the problem are compared and analysed. Finally, Section 5 concludes the article.

2. Theoretical model

In this section, an analytical model for a spherically-shaped hyperelastic balloon actuator subjected to an angular rotation with an applied internal air pressure is developed. The developed model is further used to analyse the actuation characteristics of a balloon actuator for varying pressure and rotational velocity inputs.

2.1. Problem definition

Consider a hyperelastic balloon actuator made of a thick-walled spherically-shaped polymeric material shown in Figure 2. The hyperelastic balloon actuator is assumed to be incompressible, isotropic, and homogeneous. The deformation field of the balloon actuator due to applied pressure P and angular rotation ω is assumed to preserve its spherical symmetry after the deformation.

2.2. Hyperelastic deformation

The undeformed and deformed geometries of a rotating rubber balloon actuator are described in Figure 2. The undeformed reference configuration β_0 is described in terms of spherical coordinates (R, Θ, Φ) as

$$A \leq R \leq B, 0 \leq \Theta \leq 2\pi, 0 \leq \Phi \leq 2\pi, \quad (1)$$

where A and B are the undeformed inner and outer radius of the balloon actuator, respectively. Similarly, the deformed current configuration β is described in terms of the coordinates (r, θ, ϕ) by

$$a \leq r \leq b, 0 \leq \theta \leq 2\pi, 0 \leq \phi \leq 2\pi, \quad (2)$$

where a and b are the deformed inner and outer radius of the balloon actuator, respectively. For the spherical symmetric deformation, the deformation map connecting the undeformed and deformed variables for the actuator is given by

$$r(R) = [R^3 - A^3 + a^3]^{1/3}, \theta = \Theta, \phi = \Phi, \quad (3)$$

where r is the radius at current configuration β, which was R in reference configuration β_0. The deformation gradient tensor $\mathbf{F}$ and the corresponding left-Cauchey green deformation tensor $B = FF^T$ for the given deformation map (3) are defined as

$$\mathbf{F} = \begin{bmatrix} \frac{dr}{dR} & 0 & 0 \\ 0 & \frac{r\theta}{R\Theta} & 0 \\ 0 & 0 & \frac{r\phi}{R\Phi} \end{bmatrix}, \mathbf{B} = \begin{bmatrix} \left(\frac{dr}{dR}\right)^2 & 0 & 0 \\ 0 & \frac{r^2}{R^2} & 0 \\ 0 & 0 & \frac{r^2}{R^2} \end{bmatrix}. \quad (4)$$

The corresponding principal stretches are given by

$$\lambda_r = \frac{dr}{dR}, \lambda_\theta = \lambda_\phi = \frac{r}{R}. \quad (5)$$

The above principal stretches (4) of the balloon may be related using an incompressibility condition (det $\mathbf{F} = 1$) as

$$\lambda_r \lambda_\theta \lambda_\phi = \frac{dr}{dR} \frac{r^2}{R^2} = 1. \quad (6)$$

The set of invariants corresponding to an incompressible isotropic hyperelastic material deformation are given by (Beatty 1987; Khajehsaeid, Arghavani, and Naghdabadi 2013)
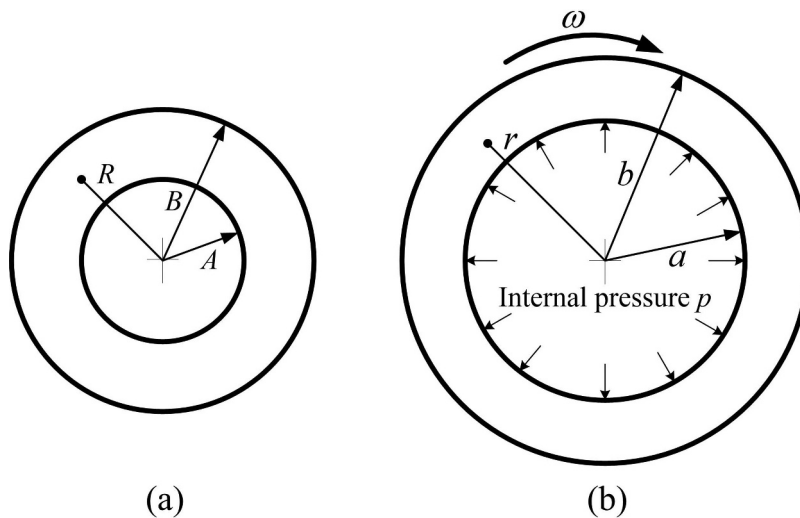
Figure 2. Nomenclature of a rubber balloon actuator: (a) Undeformed configuration (b) Deformed configuration under given rotation.

$$I_1 = \text{tr}B = \lambda_r^2 + \lambda_\theta^2 + \lambda_\phi^2, I_2 = \tfrac{1}{2}\left[(\text{tr}B)^2 - \text{tr}B^2\right] = \tfrac{1}{\lambda_r^2} + \tfrac{1}{\lambda_\theta^2} + \tfrac{1}{\lambda_\phi^2},$$
$$I_3 = \det B = \left(\lambda_r\lambda_\theta\lambda_\phi\right)^2. \tag{7}$$

2.3. Hyperelastic governing equations

In this work, we use an up to date Augmented-Gent model type of strain energy function proposed by Carrol (Carroll 2011), defined in terms of the invariants I_1 and I_2 as

$$W(I_1, I_2) = -C_1 \ln\left(\frac{I_m - I_1}{I_m - 3}\right) + C_2\sqrt{I_2}, \tag{8}$$

where C_1 term was introduced similar to Gent (Gent 1996) to enforce limiting chain extensibility through a bound on the first invariant $(I_1 < I_m)$ and the augmenting C_2 term was included specific to provide a better fit with various soft material class. These material parameters may be obtained by fitting the above energy density (8) with a well-known Treloar's uniaxial extension data for rubber similar to (Khajehsaeid, Arghavani, and Naghdabadi 2013; Mansouri and Darijani 2014). From the theory of hyperelasticity (Beatty 1987; Rivlin and Saunders 1951), the Cauchy stress tensor σ for a given invariant-based strain energy density function (8) may be expressed as

$$\sigma = \frac{2}{\sqrt{I_3}}\mathbf{B}\frac{\partial W(I_1, I_2, I_3)}{\partial \mathbf{B}} = \frac{2}{\sqrt{I_3}}\left(\frac{\partial W}{\partial I_1}\frac{\partial I_1}{\partial \mathbf{B}} + \frac{\partial W}{\partial I_2}\frac{\partial I_2}{\partial \mathbf{B}} + \frac{\partial W}{\partial I_3}\frac{\partial I_3}{\partial \mathbf{B}}\right). \tag{9}$$

The derivatives of the invariants (7) with respect to the left Cauchy green deformation tensor $\mathbf{B}$ are given by

$$\frac{\partial I_1}{\partial \mathbf{B}} = \mathbf{I}, \frac{\partial I_2}{\partial \mathbf{B}} = I_1\mathbf{I} - \mathbf{B}, \frac{\partial I_3}{\partial \mathbf{B}} = I_2\mathbf{I} - I_1\mathbf{B} + \mathbf{B}^2, \tag{10}$$

where $\mathbf{I}$ is the identity tensor. On using the above relations (9) and (10) for an incompressible balloon actuator made of hyperelastic material, we obtain

$$\sigma = -p\mathbf{I} + 2\frac{\partial W}{\partial I_1}\mathbf{B} + 2\frac{\partial W}{\partial I_2}(I_1\mathbf{B} - \mathbf{B}^2), \tag{11}$$

where p denotes the indeterminate pressure to be determined from boundary conditions. The corresponding principal Cauchy stress components are obtained using equations (8) and (11) as

$$\sigma_{rr} = -p + \left(\frac{2C_1}{I_m - I_1}\right)\frac{R^4}{r^4} - \frac{C_2}{\sqrt{I_2}}\frac{r^4}{R^4}, \sigma_{\theta\theta} = \sigma_{\phi\phi} = -p + \left(\frac{2C_1}{I_m - I_1}\right)\frac{r^2}{R^2} - \frac{C_2}{\sqrt{I_2}}\frac{R^2}{r^2}. \tag{12}$$

The material parameters $C_1 = 10.5$ MPa, $C_2 = 0.09$ MPa and $I_m = 84$ are obtained by fitting the above amended energy function (8) with a well-known Treloar's uniaxial extension data for rubber from the studies (Khajehsaeid, Arghavani, and Naghdabadi 2013; Mansouri and Darijani 2014). By employing the conservation of linear momentum principle in radial direction, the equilibrium equation for the

balloon actuator of density ρ with a rotation ω about the axis of symmetry is given by (Chadwick, Creasy, and Hart 1977; Almasi, Baghani, and Moallemi 2017)

$$\frac{d\sigma_{rr}}{dr} = \frac{2(\sigma_{\theta\theta} - \sigma_{rr})}{r} - \pi\rho\omega^2 r. \tag{13}$$

For the given boundary condition $\sigma_{rr}(r = a) = -P$ along with (12), the above equailibrium equation (13) is integrated to calculate the radial stress component as

$$\sigma_{rr} = P + \int_a^r \left[\frac{4C_1}{I_m - I_1}\left(\frac{r^2}{R^2} - \frac{R^4}{r^4}\right) - \frac{2C_2}{\sqrt{I_2}}\left(\frac{R^2}{r^2} - \frac{r^4}{R^4}\right)\right]\frac{dr}{r} - \frac{\pi\rho\omega^2}{2}(r^2 - a^2) \tag{14}$$

Further, the remaining stress components are obtained using the relations (12) given by

$$\sigma_{\theta\theta} = \sigma_{\phi\phi} = \sigma_{rr} + \frac{2C_1}{I_m - I_1}\left(\frac{r^2}{R^2} - \frac{R^4}{r^4}\right) - \frac{C_2}{\sqrt{I_2}}\left(\frac{R^2}{r^2} - \frac{r^4}{R^4}\right). \tag{15}$$

3. Finite element method-based simulation

In this section, the finite element analysis (FEA) for a rotating spherical balloon actuator is presented within the framework of hyperelasticity. A FEM-based ABAQUS 6.10 software is used to simulate the actuation model of a balloon actuator developed in the previous section for varying pressure and rotational velocity inputs.

3.1. Geometrical parameters

For the finite element analysis (FEA) of the balloon actuator, the actuator's geometry in the plane is considered a thick semi-circle under the axisymmetric assumption. Further, the thick semi-circle is reduced to a thick quarter-circle, as shown in Figure 3 using the symmetry about the horizontal x-axis. As per the limiting assumption of a thick-walled pressure vessels, the ratio of internal radius to thickness should be less than 10 $\left(i.e., \frac{r_i}{r_0 - r_i} < 10\right)$. In line with that, the undeformed dimensions of the balloon actuator for FEA are considered as $A = 0.3$ m and $B = 0.5$ m. For the given dimensions, an axisymmetric deformable shell geometry of the thick quarter-circle shown in Figure 3 is constructed.

3.2. Material properties

In this work, we select the neoprene type of synthetic rubber (Mansouri and Darijani 2014) for the analysis because it resists degradation better than the natural rubber. Neoprene rubber is assumed to be a homogeneous, incompressible, and hyperelastic material for this study. The finite element solver requires the density and the hyperelastic material model. ABAQUS 6.10 only has inbuilt strain energy functions like Neo-Hookean, Mooney-Rivlin,

Ogden, and Yeoh. Thus, a user-defined subroutine is used to accurately model the hyperelastic properties of Neoprene with the Augmented-Gent Model. Earlier study (Almasi, Baghani, and Moallemi 2017) have also employed an exp-exp model instead of readily available inbuilt strain energy functions in ABAQUS 6.10 to obtain good accuracy. A UHYPER subroutine is used to define the Augmented-Gent strain energy density function for isotropic hyperelastic material behaviour. The UHYPER subroutine is coded in FORTRAN, and it requires the derivatives of strain energy density function with respect to the strain invariants. The UHYPER subroutine takes three constants C_1, C_2, and I_m as input, which is calculated by fitting the Augmented-Gent material model with the Treloar's experimental data from the studies (Khajehsaeid, Arghavani, and Naghdabadi 2013; Mansouri and Darijani 2014).

3.3. Load and boundary conditions

A load of pressure P is applied to the inner surface QR for carrying out the FEM analysis of a spherical balloon actuator. An additional rotational body force is applied to a rotating balloon actuator. The actuator rotates the thick quarter-circle with an angular velocity, ω around the vertical y-axis, as shown in Figure 3. The boundary conditions required to define the FEM are YSYMM (U2 = UR1 = UR3 = 0) about RS to restrict the change of y-coordinate and XSYMM (U1 = UR2 = UR3 = 0) about PQ to restrict the change of x-coordinate, as shown in Figure 3(a).

3.4. Element type and mesh sensitivity

Considering the symmetry of the model, a structured quad element shape is selected to mesh the part geometry. An 8-node biquadratic axisymmetric quadrilateral, hybrid, linear pressure (CAX8H) element type is selected from the axisymmetric stress family. Mesh sensitivity analysis for the finite-element model is carried out based on the convergence of minimum radial and hoop values stresses to a stationary value by varying the number radial and hoop divisions of the geometry. The optimum mesh is attained at 20 divisions along the radius and 80 divisions along the circumference, with 1600 elements and 5001 nodes as shown in Figure 3(b). The detailed mesh-sensitivity study is carried out by varying different process parameters. However, for the sake of brevity, those results are not reported here.

3.5. FEM simulation-based outer deformed radius evaluation

The developed analytical model first requires the specification of the deformed inner or outer radius to obtain the stress distributions in the balloon actuator. The deformed inner radius can be obtained from the relation (3) $_1$ using the constant volume assumption (6) after specifying the deformed outer diameter from FEA or vice-versa. In this context, the data points of internal pressure P with the deformed outer radius b extracted from FEA are shown in Figure 4 for the actuator at different internal pressure forces. A 2-degree exponential curve fit is also obtained here to specify the deformed outer radius at a given internal pressure. The corresponding equation of 2-degree exponential curve is given by
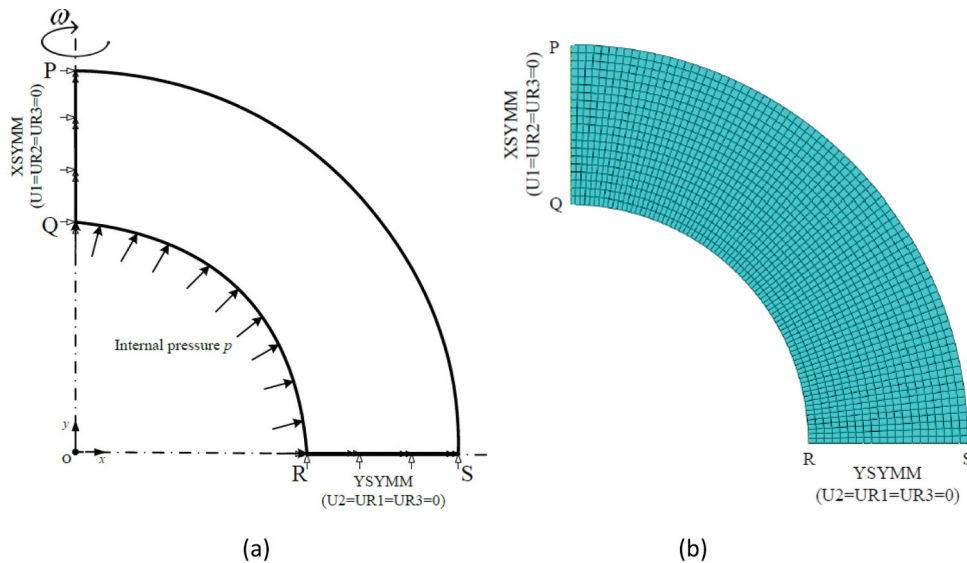

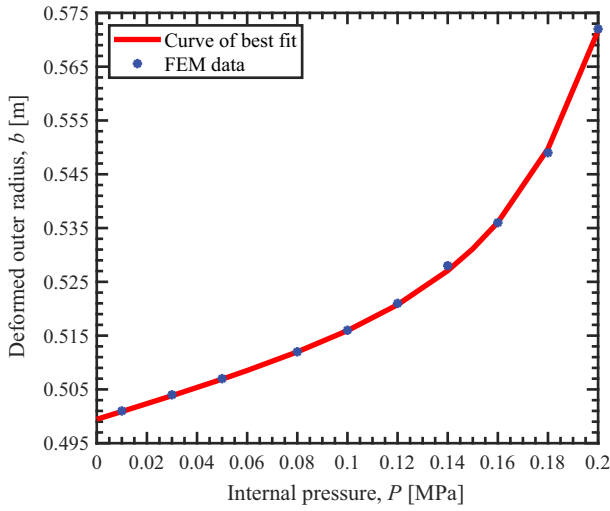Figure 3. The 2-D axisymmetric modelling for FEM simulation: (a) Model with boundary conditions (b) Mesh network.

Figure 4. Effect of the internal pressure variation on the deformed outer radius in a rubber balloon actuator.

$$b = 0.4993e^{0.2781p} + 0.0001481e^{28.45p}. \tag{16}$$

4. Comparison of analytical results with FEM simulation

In this section, the rubber balloon actuator model presented in Section 2 is utilised to analyse the actuation outputs by varying P, ω, and t. The analytical solutions based on the developed actuation model for a thick-walled spherically-shaped rubber balloon actuator are verified with the FEM simulation-based results. In addition, various elastic instability curves are also obtained for both with and without rotation cases to examine critical inflation states of the actuator. The actuator's geometry is considered as follows: inner radius A is 300 mm, outer radius B is 500 mm, thickness t is 200 mm. The pressure $P = 0.1$ MPa is applied at the

actuator's inner periphery, and the outer edge is at ambient pressure. By applying the internal pressure, the thickness of the spherically-shaped balloon actuator is reduced, and the actuator's surface area is increased at the deformed state. The radial stress, σ_r and hoop stresses, $\sigma_\theta = \sigma_\phi$ at different radial locations of the deformed shape of the actuator are studied.

4.1. Stresses in the rubber balloon actuator with and without rotation

Figure 5 presents the radial and hoop stress plots at a different non-dimensional radial distance by analytical and FEM for both rotary ($\omega = 40$ rpm and 80 rpm) and stationary conditions of the actuator. The analytical solutions obtained using the Augmented-Gent model (8) and the FEM results obtained from ABAQUS software are in good agreement. It is to be noticed from Figure 5(a) that the radial stress is varied from 0 to 0.1 MPa in compression from the outer to inner periphery of the actuator. This corresponds to the imposed boundary and loads applied conditions. An increment in radial stress to reach zero at the deformed outer radius is observed in both the rotary and stationary states. However, a decrement in the hoop stress from the maximum at inner radius to the minimum at outer radius is noted in Figure 5(b). A variation on the radial and hoop stresses along the thickness direction at different angular velocities (ω= 0, 40, and 80 rpm) can be noted by analytical and FEM. With an increase in the angular speed ω, a significant increment in radial and hoop stresses is obtained. The rotational effect on the distribution of radial and hoop stresses is pronounced near the inner periphery compared to the actuator's outer periphery. This is because the inner periphery imposed the internally applied pressure, whereas the outer
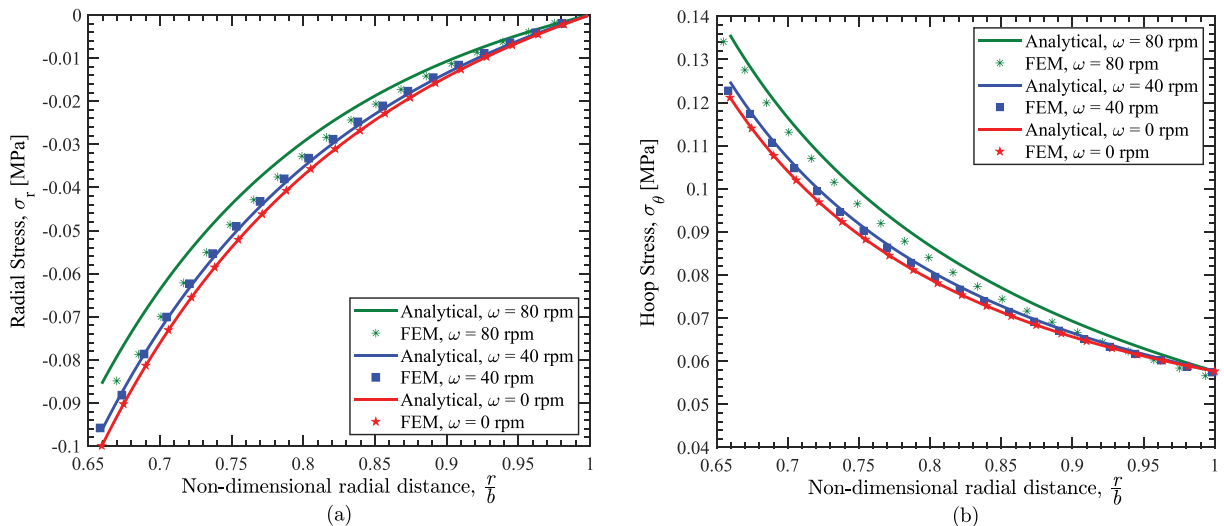

Figure 5. The distribution of (a) radial stress and (b) hoop stress in a rubber balloon actuator at $\omega = 0$ rpm, 40 rpm, and 80 rpm.

periphery is in an open environment. Also, one may note the slight deviation between the analytical and FEM simulation results at higher rotation. This is because the element of FEM model is used as massless and results in the discrete distribution of centrifugal force. On the other hand, the analytical model considers the continuous centrifugal force distribution. Despite the mass sensitivity test, we can not avoid the mass lumping in the FEM model. Finally, the FEM results, though very nearly match with the analytical results.

4.2. Varying the internal pressure in the actuator with and without rotation

Figures 6, 7 present the radial and hoop stress plots at three different levels of internal pressure by analytical and FEM for both rotary ($\omega = 80$ rpm) and stationary

conditions of the actuator, respectively. It is to be noted that the deformed radius of the actuator decreases with an increase in the applied pressure. As a result, the radial and hoop stress patterns differ at different applied pressure P in both the actuator's rotary and stationary states. With an increase in the internal pressure P from 0.05 to 0.1 MPa, a significant increment in radial and hoop stresses is observed. However, the radial and hoop stress patterns with radial locations become flatter and steeper, respectively, when pressure is increased from 0.05 to 0.15 MPa. Also, these patterns of radial and hoop stress with radial locations are monotonic with the rotational effect. However, the magnitude of radial and hoop stresses is increased in all cases of $\omega = 0$ rpm and 80 rpm rotation. In addition, a slight deviation in analytical and FEM results for radial stress is observed as the effect of rotation is quite large due to mass
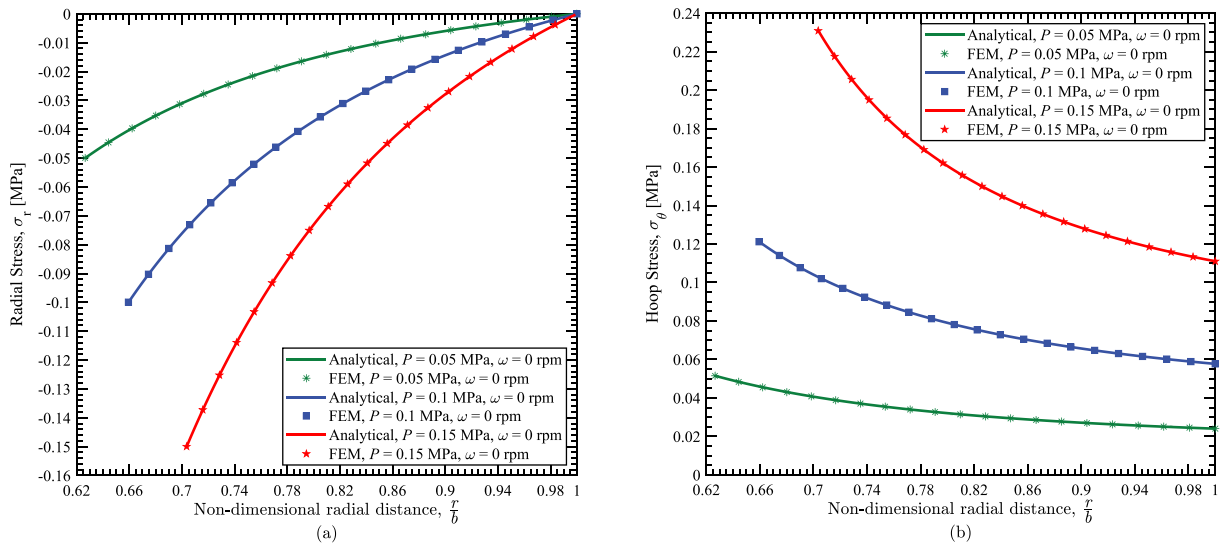

Figure 6. The distribution of (a) radial stress and (b) hoop stress in a stationary rubber balloon actuator with different internal pressures.
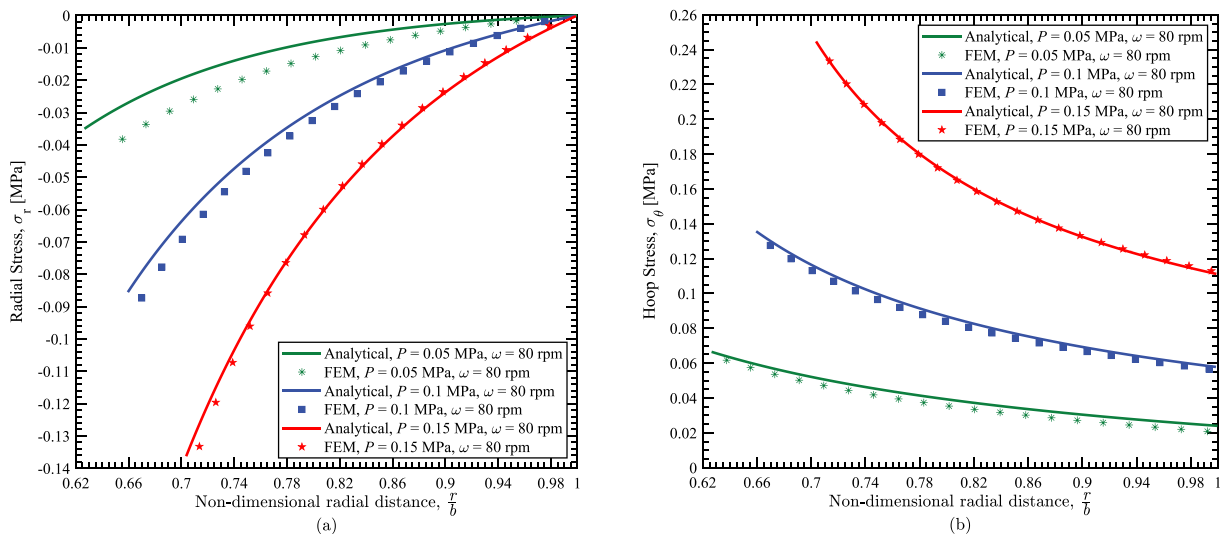

Figure 7. The distribution of (a) radial stress and (b) hoop stress in a rotary rubber balloon actuator with different internal pressures.

lumping than the external pressure. Over here, the pressure is dominating. However, for the hoop stress, the impact of mass lumping is negligible.

4.3. Varying the thickness of the rubber actuator with and without rotation

Figures 8, 9 present the radial and hoop stress plots at three different levels of thickness by analytical and FEM for both rotary ($\omega = 80$ rpm) and stationary conditions of the actuator, respectively. One may note that radial stress profiles here become approx linear when the actuator's thickness is increased from 0.1 to 0.3 m while keeping the same inner radius. On the other hand, the hoop stress profiles with the radial locations become steeper at similar conditions. This suggests that the proper selection of thickness plays a significant role in the performance of the actuator. A similar variation on the radial and hoop

stresses at different angular velocities ($\omega = 0$ and 80 rpm) is also noted here again, like previous internal pressure variation situations by analytical and FEM. Also, at higher rotation, a slight deviation in radial stress between the analytical and FEM simulation results is observed. This is because the effect of mass lumping in FEM model is dominated as the thickness increases. However, for the hoop stress, the impact of mass lumping is negligible, so the FEM and analytical results matched perfectly.

4.4. Elastic instability curves for a thick rubber balloon actuator with and without rotation

In the ongoing problem, a rotating balloon actuator is internally pressurised with an applied pressure P. The actuator's material is assumed to be an incompressible, isotropic, and hyperelastic material that can sustain the large elastic deformations. For a given applied pressure
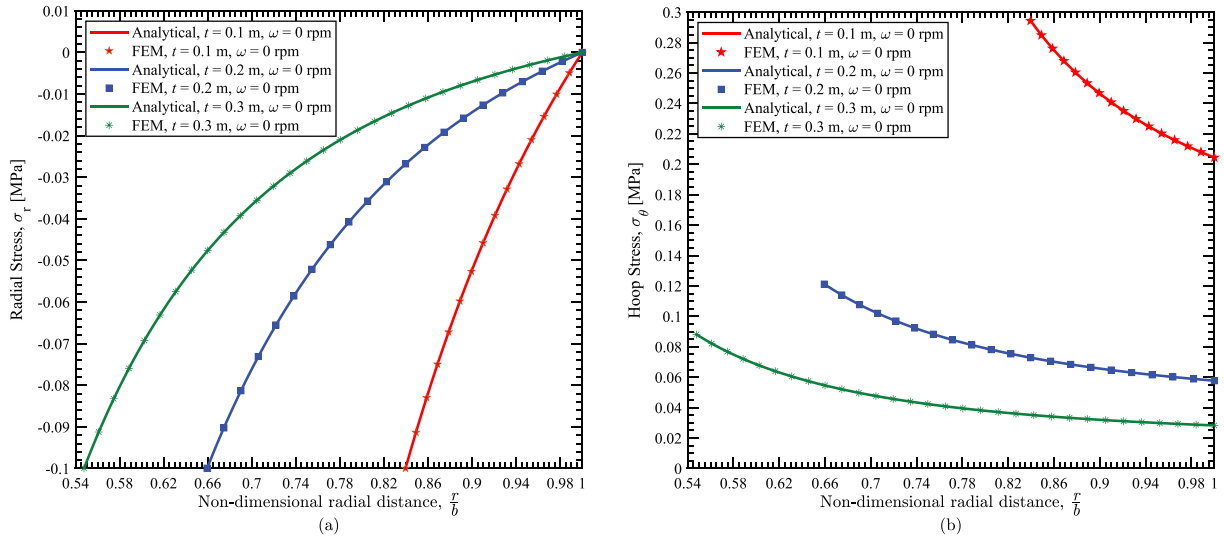

Figure 8. The distribution of (a) radial stress and (b) hoop stress in a stationary rubber balloon actuator with different thicknesses.
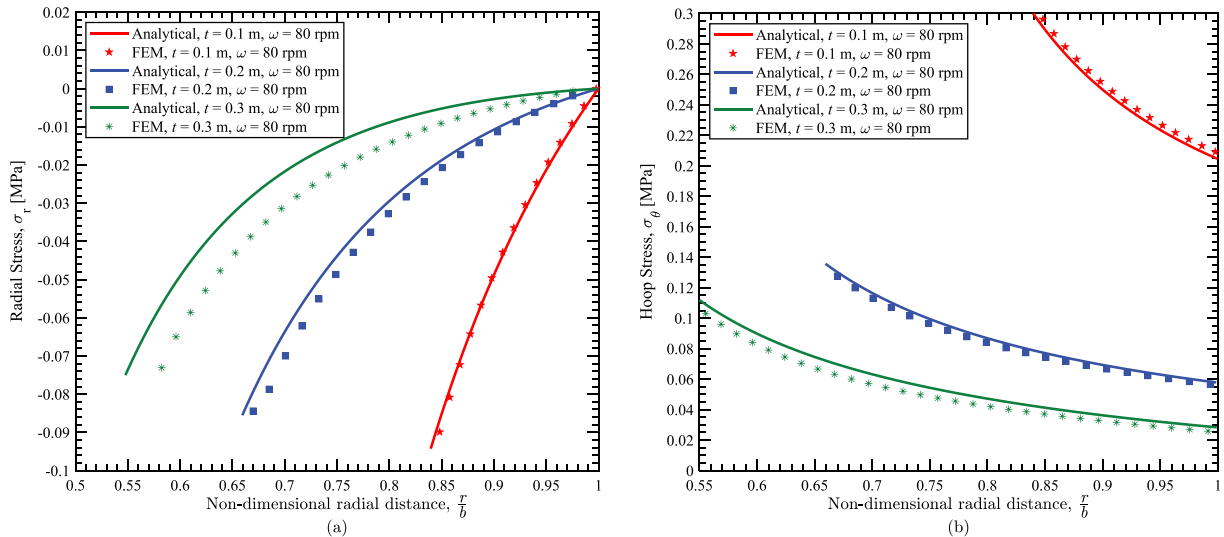

Figure 9. The distribution of (a) radial stress and (b) hoop stress in a rotary rubber balloon actuator with different thicknesses.

P, the balloon material may undergo large elastic deformations that exhibit novel instabilities. These instabilities in the actuator can be observed in the form of aneurysm formation, non-uniform stretching, and small cavities expansion when the actuator reached a critical inflation state. For the detailed elastic instabilities analysis of the balloon actuator without rotation, we refer to a well-known study by Gent (Gent 2005) and references therein. However, the elastic instability analysis of the balloon actuator with and without rotation is explored here to examine critical inflation states by obtaining the various elastic instability curves. In this context, the equilibrium equation (13) with the suitable boundary conditions is utilised. On integrating the equilibrium equation (13) for the given boundary conditions $\sigma_{rr}(r = a) = -P$ and $\sigma_{rr}(r = b) = 0$ along with (12), we obtain

$$\int_{\sigma_{rr}(a)=-P}^{\sigma_{rr}(b)=0} d\sigma_{rr} = \int_{a}^{b} \left[\frac{4C_1}{I_m - I_1} \left(\frac{r^2}{R^2} - \frac{R^4}{r^4} \right) - \frac{2C_2}{\sqrt{I_2}} \left(\frac{R^2}{r^2} - \frac{r^4}{R^4} \right) - \pi\rho\omega^2 r^2 \right] \frac{dr}{r}$$

(17)

To simplify the above integral equation (17), a Jacbian $\frac{dr}{r} = \frac{d\lambda}{\lambda(1-\lambda^3)}$ obtained from the defined parameter $\lambda = \frac{r}{R}$ called stretch is utilised. On using the defined Jacobian, the above integral equation (17) is rewritten as

$$P = \int_{\lambda_a}^{\lambda_b} \left[\frac{4C_1}{I_m - I_1} \left(\lambda^2 - \frac{1}{\lambda^4} \right) - \frac{2C_2}{\sqrt{I_2}} \left(\frac{1}{\lambda^2} - \lambda^4 \right) - \pi\rho\omega^2\lambda^2 R^2 \right] \frac{d\lambda}{\lambda(1-\lambda^3)}$$

(18)

where $\lambda_a = a/A$ and $\lambda_b = b/B$. A numerical solution of the above equation (18) for the given material parameters $C_1 = 10.5$ MPa, $C_2 = 0.09$ MPa, and $I_m = 84$, is used to obtain the elastic instability curves to examine the critical inflation of the rubber balloon actuator (Khajehsaeid, Arghavani, and Naghdabadi

2013; Mansouri and Darijani 2014). eEquation (18) is numerically integrated using global adaptive quadrature (Gander and Gautschi 2000).

Figure 10 compares the limiting chain extensibility I_m parameter effect enforced on the (P versus λ_a) and (P versus λ_b) instability curves obtained analytically and by FEM simulation. It can be seen that the analytical instability curves match with the FEM simulation results to or less than the critical pressure. Beyond the critical pressure, the FEM-based software ABAQUS 6.10 cannot run the simulations, and it shows the convergence and too many increment errors. These errors may be because FEM-based software ABAQUS 6.10 employed the implicit formulation dealing with large elastic deformation problems. It is noted that the provision is available in ABAQUS 6.10 software to check the stability of the stress-strain data of the specific materials. Consequently, the FEM simulations are plotted up to the critical pressure and compared with analytical results. A significant variation in the parameter I_m affects the actuator's critical inflation state shown in the elastic insatiability curves. The interpretation of pressure with stretches λ_a and λ_b follows a similar pattern, which is favourable for improved accuracy and stability of the balloon actuator under loading conditions. Both stretch λ_a and λ_b can be used as a designing parameter for balloon actuators. Also, the analytical findings of the instability model (18) to plot the instability curves at zero rotation may be examined and correlated for the existing configurations of the balloon actuators (Alexander 1971; Needleman 1977; Sharma, Arora, and Joglekar 2018).

After validating the actuator's critical inflation with FEM simulation, the rotational effect on the elastic instability curves is studied at different angular velocities analytically. In line with that, a critical pressure decrement is observed with an increase in the rotational speed from $\omega = 0$ to 160 rpm as shown in Figure 11.
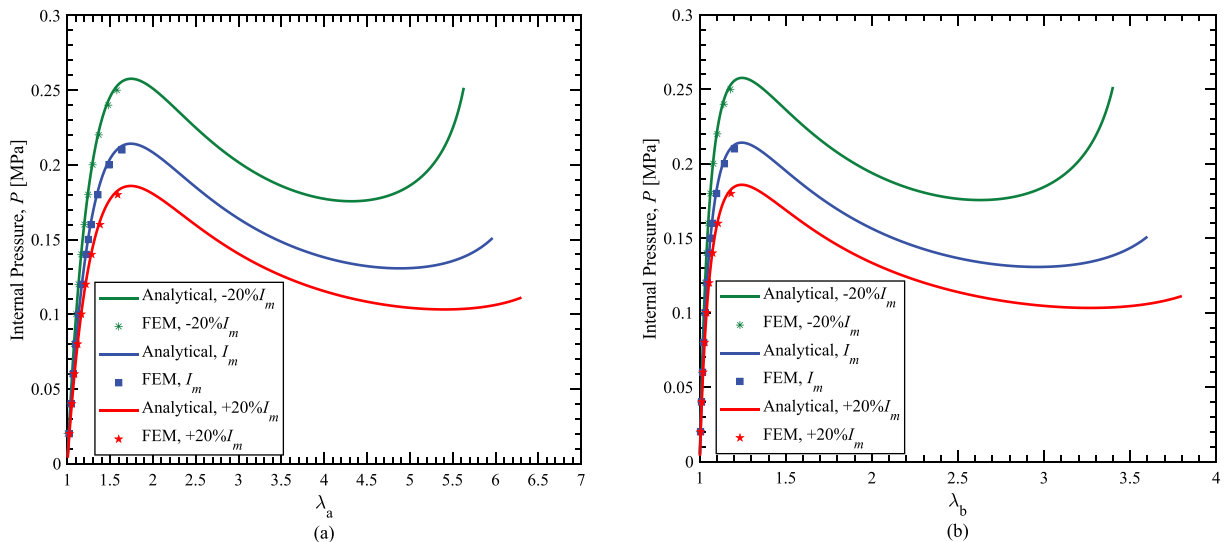

Figure 10. Elastic instability curves for a stationary thick rubber balloon actuator with different chain extensibility parameters.
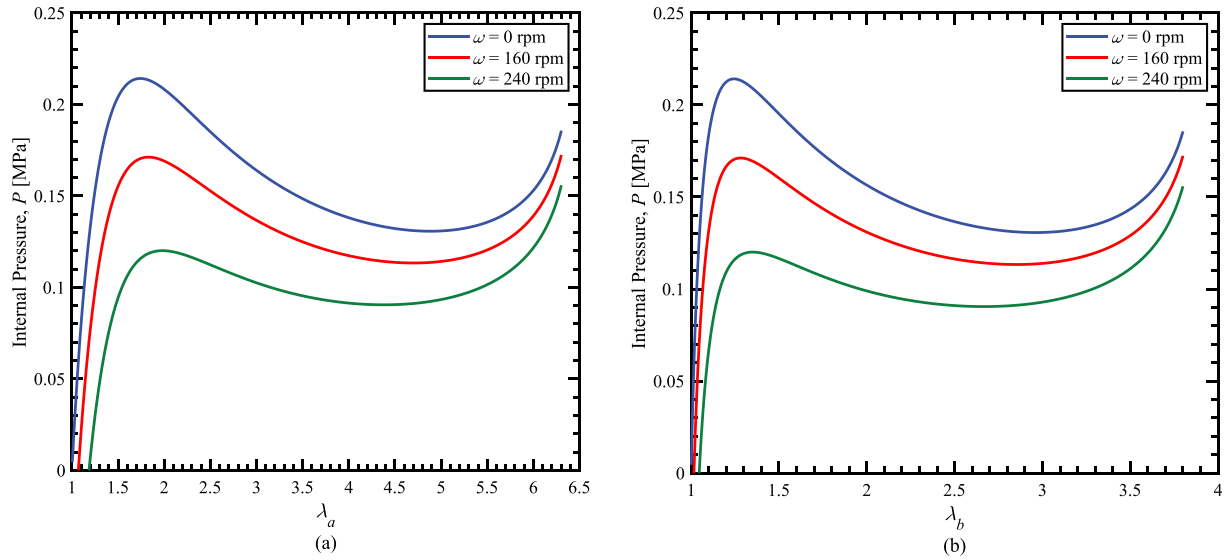
Figure 11. Elastic instability curves for a thick rubber balloon actuator at $\omega = 0$ rpm, 160 rpm, and 240 rpm.

This is because the effect of centrifugal force during rotation dominates the actuator's elastic instability. Further, it is observed that a critical pressure decrement increases with increasing ω from 160 to 240 rpm. At last, the pattern of instability curves with stretches λ_a and λ_b are approximately the same.

5. Conclusions

In this work, a thermodynamically consistent modelling and a computationally efficient FEM simulation are presented for a rubber balloon actuator subjected to an angular rotation with an internally applied air pressure. The model is developed to predict the response of the actuator for a given angular rotation with internally applied air pressure. The model is utilised to perform the parametric studies for varying input parameters of the actuator. The proposed analytical material model and FEM simulation are compared and found to be satisfactorily matching with each other. The critical inflation limits for the actuator are also examined from the elastic instability curves for the given angular rotation. A given rotational effect to the balloon actuator enhanced the radial and hoop stress magnitudes and reduced the actuator's critical inflation limit. The significant contribution of the present study is an attempt to explore the rotational effect of the rubber balloon actuator in the soft robotics field, which is generally ignored. The previous parallel results in the literature can also be obtained from the current study as a special case of the present one. The current work may be further explored in developing a thermodynamically consistent and FEM-based model solution to predict the temperature response on the balloon actuator. The potential future applications of such model situations lie in designing of spherical rovers for planetary exploration working under extreme environmental conditions.

Disclosure statement

No potential conflict of interest was reported by the author(s).

Notes on contributors

Dr. Vinod Yadav is an Assistant Professor in the Department of Mechanical Engineering at MANIT-Bhopal. Dr. Yadav received his Ph.D. in Mechanical Engineering (Specialized in Design & Manufacturing) from IIT-Guwahati in 2016. His main areas of interest include Solid Mechanics, FEM, and Plasticity.

Dr. Deepak Kumar is an Assistant Professor in the Department of Mechanical Engineering at MANIT-Bhopal. Prior to joining MANIT-Bhopal, he worked as a Postdoctoral Fellow with a research group on bio-mechanics and soft machines at Applied Mechanics Department of IIT-Delhi. He also worked as a Research Associate at SRIC-IIT Kharagpur. Dr. Kumar received his Ph.D. in Mechanical Engineering (Specialized in Continuum Mechanics) from IIT-Patna in 2019. His main areas of interest include Soft Materials Mechanics, Electro-magneto-elasticity, and Electro-magneto-rheology. Dr. Kumar is a highly motivated dynamic scholar and fully dedicated to the original research. He regularly writes and reviews articles for various peer-reviewed international journals and conferences.

Ayush Srivastav is a final year undergraduate student in the Department of Mechanical Engineering at MANIT, Bhopal, India.

Dr. Somnath Sarangi is a professor in the Department of Mechanical Engineering at IIT Patna.

ORCID

Deepak Kumar http://orcid.org/0000-0001-9048-8828

Data Availability Statement (DAS)

The authors accept the publicly available data sharing policy, under which all authors are required to make the data and materials that support the results or analyses presented in their paper freely available.

References

Albu-Schaffer, A., O. Eiberger, M. Grebenstein, S. Haddadin, C. Ott, T. Wimbock, S. Wolf, and G. Hirzinger. 2008. "Soft Robotics." *IEEE Robotics & Automation Magazine* 15 (3): 20–30. doi:10.1109/MRA.2008.927979.

Alexander, H. 1971. "Tensile Instability of Initially Spherical Balloons." *International Journal of Engineering Science* 9 (1): 151–160. doi:10.1016/0020-7225(71)90017-6.

Almasi, A., M. Baghani, and A. Moallemi. 2017. "Thermomechanical Analysis of Hyperelastic Thickwalled Cylindrical Pressure Vessels, Analytical Solutions and Fem." *International Journal of Mechanical Sciences* 130: 426–436. doi:10.1016/j.ijmecsci.2017.06.033.

An, Z., and Y. Lu. 2005. "A Numerical Model for Micro Balloon-jointed Actuation." In *ASME 2005 International Mechanical Engineering Congress and Exposition*, 295–300. American Society of Mechanical Engineers Digital Collection.

Andersen, T. O., and M. R. Hansen. 2005. "Applications of Modelling and Simulation in Mechatronics and Fluid Power System Design-education and Research." *Australian Journal of Mechanical Engineering* 2 (2): 93–103. doi:10.1080/14484846.2005.11464483.

Ashwin, K., and A. Ghosal. 2019. "Static Modeling of Miniaturized Pneumatic Artificial Muscles, Kinematic Analysis, and Experiments on an Endoscopic End-effector." *IEEE/ASME Transactions on Mechatronics* 24 (4): 1429–1439. doi:10.1109/TMECH.2019.2916783.

Beatty, M. F. 1987. *Topics in Finite Elasticity: Hyperelasticity of Rubber, Elastomers, and Biological Tissues|with Examples.* ASME.

Blatz, P. J., and W. L. Ko. 1962. "Application of Finite Elastic Theory to the Deformation of Rubbery Materials." *Transactions of the Society of Rheology* 6 (1): 223–252. doi:10.1122/1.548937.

Carroll, M. 2011. "A Strain Energy Function for Vulcanized Rubbers." *Journal of Elasticity* 103 (2): 173–187. doi:10.1007/s10659-010-9279-0.

Chadwick, P., C. Creasy, and V. Hart. 1977. "The Deformation of Rubber Cylinders and Tubes by Rotation." *The ANZIAM Journal* 20 (1): 62–96.

Fung, Y. 1967. "Elasticity of Soft Tissues in Simple Elongation." *American Journal of Physiology- Legacy Content* 213 (6): 1532–1544. doi:10.1152/ajplegacy.1967.213.6.1532.

Gander, W., and W. Gautschi. 2000. "Adaptive Quadrature| revisited." *BIT Numerical Mathematics* 40 (1): 84–101. doi:10.1023/A:1022318402393.

Gent, A. N. 1996. "A New Constitutive Relation for Rubber." *Rubber Chemistry and Technology* 69 (1): 59–61. doi:10.5254/1.3538357.

Gent, A. 2005. "Elastic Instabilities in Rubber." *International Journal of Non-Linear Mechanics* 40 (2–3): 165–175. doi:10.1016/j.ijnonlinmec.2004.05.006.

He, Q., Y. Zheng, Z. Wang, X. He, and S. Cai. 2020. "Anomalous Inflation of a Nematic Balloon." *Journal of the Mechanics and Physics of Solids* 142: 104013. doi:10.1016/j.jmps.2020.104013.

Hwang, Y., O. H. Paydar, and R. N. Candler. 2015. "Pneumatic Microfinger with Balloon Fins for Linear Motion Using 3d Printed Molds." *Sensors and Actuators. A, Physical* 234: 65–71. doi:10.1016/j.sna.2015.08.008.

Jebur, Q., M. J. Jweeg, and M. Al-Waily. 2021. "Ogden Model for Characterising and Simulation of Pphr Rubber under Different Strain Rates." *Australian Journal of Mechanical Engineering* 1–15. doi:10.1080/14484846.2021.1918375.

Jeong, O. C., S. Kusuda, and S. Konishi. "All Pdms Pneumatic Balloon Actuators for Bidirectional Motion of Micro Finger." in: 18th IEEE International Conference on Micro Electro Mechanical Systems, 2005. MEMS 2005, Japan, IEEE, 2005, 407–410.

Jeong, O. C., S. Kusuda, T. Sakakibara, S. Konishi, and M. Nokata. "Pneumatic Micro Finger as Endeffecter of Robot." in: IEEE International Symposium on Micro-NanoMechatronics and Human Science, 2005, Nagoya, Japan, IEEE, 2005, 145–148.

Kanner, L. M., and C. O. Horgan. 2007. "Elastic Instabilities for Strain-stiffening Rubber-like Spherical and Cylindrical Thin Shells under Inflation." *International Journal of Non-Linear Mechanics* 42 (2): 204–215. doi:10.1016/j.ijnonlinmec.2006.10.010.

Khajehsaeid, H., J. Arghavani, and R. Naghdabadi. 2013. "A Hyperelastic Constitutive Model for Rubber-like Materials." *European Journal of Mechanics-A/Solids* 38: 144–151. doi:10.1016/j.euromechsol.2012.09.010.

Kumar, D., S. Ghosh, S. Roy, and S. Santapuri. 2021. "Modeling and Analysis of an Electro-pneumatic Braided Muscle Actuator." *Journal of Intelligent Material Systems and Structures* 32 (4): 399–409. doi:10.1177/1045389X20953624.

Lee, G.-B., Y.-C. Tai, C. Grosjean, and C.-M. Ho. "Application of Micromachined Balloon Actuators on Control of Leading-edge Vortices of a Delta Wing." in: Proc. 22nd National Conference on Theoretical and Applied Mechanics, US, 1998.

Lu, Y., and C.-J. Kim. "Micro-finger Articulation by Pneumatic Parylene Balloons." in: TRANSDUCERS' 03. 12th International Conference on Solid-State Sensors, Actuators and Microsystems. Digest of Technical Papers (Cat. No. 03TH8664), Boston, MA, USA, Vol. 1, IEEE, 2003a, 276–279.

Lu, Y., and C.-J. Kim. 2003b. "Characterization of Balloon-jointed Micro-fingers." In *ASME International Mechanical Engineering Congress and Exposition*, 311–316. Vol. 37211. Washington, DC, USA.

Mansouri, M., and H. Darijani. 2014. "Constitutive Modeling of Isotropic Hyperelastic Materials in an Exponential Framework Using a Self-contained Approach." *International Journal of Solids and Structures* 51 (25–26): 4316–4326. doi:10.1016/j.ijsolstr.2014.08.018.

Mao, G., T. Li, Z. Zou, S. Qu, and M. Shi. 2014. "Prestretch Effect on Snap-through Instability of Short-length Tubular Elastomeric Balloons under Inflation." *International Journal of Solids and Structures* 51 (11–12): 2109–2115. doi:10.1016/j.ijsolstr.2014.02.013.

Moskvichev, E., A. Porokhin, and I. Shcherbakov. "Numerical Modeling of the Strain of Elastic Rubber Elements." in: Journal of Physics: Conference Series, Tomsk, Russian Federation, Vol. 919, IOP Publishing, 2017, 012014.

Needleman, A. 1977. "Inflation of Spherical Rubber Balloons." *International Journal of Solids and Structures* 13 (5): 409–421. doi:10.1016/0020-7683(77)90036-1.

Nicholson, D. W., and N. W. Nelson. 1990. "Finite-element Analysis in Design with Rubber." *Rubber Chemistry and Technology* 63 (3): 368–406. doi:10.5254/1.3538262.

Noritsugu, T. "Pneumatic Soft Actuator for a Human-friendly Actuation System." in: Proceedings of the JFPS International Symposium on Fluid Power, Japan, Vol. 1999, Japan Fluid Power System Society, 1999, 605–610.

Ogden, R. 1982. "Elastic Deformations of Rubberlike Solids." In *Mechanics of Solids*, 499–537. Elsevier. doi:10.1016/B978-0-08-025443-2.50021-5.

Rivlin, R. 1948. "Large Elastic Deformations of Isotropic Materials. Ii. Some Uniqueness Theorems for Pure, Homogeneous Deformation, Philosophical Transactions of the Royal Society of London." *Series A, Mathematical and Physical Sciences* 240 (822): 491–508.

Rivlin, R. 1949. "Large Elastic Deformations of Isotropic Materials. V. The Problem of Flexure." *Proceedings of the Royal Society of London. Series A, Mathematical and Physical Sciences* 195 (1043): 463–473.

Rivlin, R. S., and D. Saunders. 1951. "Large Elastic Deformations of Isotropic Materials Vii. Experiments on the Deformation of Rubber, Philosophical Transactions of the Royal Society of London." *Series A, Mathematical and Physical Sciences* 243 (865): 251–288.

Saga, N., J.-y. Nagase, and T. Saikawa. "Development of a Tendon Driven System Using a Pneumatic Balloon." in: IEEE International Conference Mechatronics and Automation, 2005, Niagara Falls, ON, Canada, Vol. 2, IEEE, 2005, 1087–1092.

Sharma, A. K., N. Arora, and M. Joglekar. 2018. "Dc Dynamic Pull-in Instability of a Dielectric Elastomer Balloon: An Energy-based Approach." *Proceedings of the Royal Society A: Mathematical, Physical and Engineering Sciences* 474 (2211): 20170900. doi:10.1098/rspa.2017.0900.

Sheng, Z., F. Xiang, Z. Shouqiang, and D. Kai. 2014. "Kinetic Model for a Spherical Rolling Robot with Soft Shell in a Beeline Motion." *Journal of Multimedia* 9 (2): 223.

Simon, C. M., and C. Carraro. 2019. "Multi-and Instabilities in Gas Partitioning between Nanoporous Materials and Rubber Balloons." *Proceedings of the Royal Society A* 475 (2222): 20180703. doi:10.1098/rspa.2018.0703.

Treloar, L. R. 1974. "The Mechanics of Rubber Elasticity." In *Journal of Polymer Science: Polymer Symposia*. Vol. 48, 107–123. Wiley Online Library.doi:10.1002/polc.5070480110.

Treloar, L. R. 1976. "The Mechanics of Rubber Elasticity." *Proceedings of the Royal Society of London. A. Mathematical and Physical Sciences* 351 (1666): 301–330.

Valavala, P. K., and G. M. Odegard. 2021. Predicting Mechanical Properties Using Continuum Mechanics-Based Approach: Micro-mechanics and Finite Element Analysis. In *Theory and Modeling of Polymer Nanocomposites*, edited by Ginzburg, V. V, Hall, L. M. 310 vols. Springer, Cham: Springer Series in Materials Science. doi:10.1007/978-3-030-60443-1_8.

Verl, A., A. Albu-Schaffer, O. Brock, and A. Raatz. 2015. *Soft Robotics*. Berlin, Heidelberg: Springer.

Wang, T., F. Xu, Y. Huo, and M. Potier-Ferry. 2018. "Snap-through Instabilities of Pressurized Balloons: Pear-shaped Bifurcation and Localized Bulging." *International Journal of Non-Linear Mechanics* 98: 137–144. doi:10.1016/j.ijnonlinmec.2017.10.017.

Zamani, V., and T. J. Pence. 2017. "Swelling, Inflation, and a Swelling-burst Instability in Hyperelastic Spherical Shells." *International Journal of Solids and Structures* 125: 134–149. doi:10.1016/j.ijsolstr.2017.07.010.